Developmental Cell
Article

Structural Insights into the Organization of the Cavin Membrane Coat Complex

Oleksiy Kovtun,[1] Vikas A. Tillu,[1] WooRam Jung,[1] Natalya Leneva,[1] Nicholas Ariotti,[1] Natasha Chaudhary,[1] Ramya A. Mandyam,[1,4] Charles Ferguson,[1] Garry P. Morgan,[2] Wayne A. Johnston,[1] Stephen J. Harrop,[3,5] Kirill Alexandrov,[1] Robert G. Parton,[1,2,*] and Brett M. Collins[1,*]
[1]Institute for Molecular Bioscience, The University of Queensland, St. Lucia, QLD 4072, Australia
[2]Centre for Microscopy and Microanalysis, The University of Queensland, St. Lucia, QLD 4072, Australia
[3]School of Physics, The University of New South Wales, Sydney, NSW 2052, Australia
[4]Present address: Diamantina Institute, The University of Queensland, Woolloongabba, QLD 4102, Australia
[5]Present Address: Australian Synchrotron, Clayton, VIC 3168, Australia
*Correspondence: r.parton@imb.uq.edu.au (R.G.P.), b.collins@imb.uq.edu.au (B.M.C.)
http://dx.doi.org/10.1016/j.devcel.2014.10.002

SUMMARY

Caveolae are cell-surface membrane invaginations that play critical roles in cellular processes including signaling and membrane homeostasis. The cavin proteins, in cooperation with caveolins, are essential for caveola formation. Here we show that a minimal N-terminal domain of the cavins, termed HR1, is required and sufficient for their homo- and hetero-oligomerization. Crystal structures of the mouse cavin1 and zebrafish cavin4a HR1 domains reveal highly conserved trimeric coiled-coil architectures, with intersubunit interactions that determine the specificity of cavin-cavin interactions. The HR1 domain contains a basic surface patch that interacts with polyphosphoinositides and coordinates with additional membrane-binding sites within the cavin C terminus to facilitate membrane association and remodeling. Electron microscopy of purified cavins reveals the existence of large assemblies, composed of a repeating rod-like structural element, and we propose that these structures polymerize through membrane-coupled interactions to form the unique striations observed on the surface of caveolae in vivo.

INTRODUCTION

Caveolae are nanoscale (~60–80 nm) invaginated domains of the plasma membrane with important roles in lipid metabolism, cell signaling and trafficking, developmental processes, mechnosensation, and mitigation of mechanical stress (reviewed in Parton and del Pozo, 2013). Their high abundance on the plasmalemma of certain cell types and remarkable flask-shaped morphology allowed their discovery during the dawn of cellular electron microscopy (EM; Palade, 1953; Yamada, 1955). However, molecular characterization of caveolae only began two decades later with the identification of a membrane-embedded protein, caveolin, required for caveolae formation (Fra et al., 1995; Rothberg et al., 1992). Recently, a family of cytoplasmic proteins, the cavins, has been shown to be a second indispensible protein component of the caveola coat (Bastiani et al., 2009; Hill et al., 2008; Liu et al., 2008; McMahon et al., 2009). Mutations in both caveolins and cavins lead to diseases including cardiovascular disorders, lipodystrophy and skeletal muscular dystrophies (Parton and del Pozo, 2013).

In mammals, there are three isoforms of the integral membrane caveolins (CAV1, 2, and 3), and four members of the peripheral membrane cavin proteins (Cavin1, 2, 3, and 4) (Bastiani et al., 2009; Hansen et al., 2013; Hill et al., 2008; Liu et al., 2008). Whereas low-resolution EM studies have identified a striated caveola coat (Gambin et al., 2014; Ludwig et al., 2013; Peters et al., 1985; Rothberg et al., 1992; Westermann et al., 2005), the specific contributions of each family of proteins to caveolar coat formation are poorly understood, and the structural details unknown. Although the formation of caveolae in mammalian cells requires both caveolin and cavin proteins, recent work showed that CAV1 expression by itself in a model prokaryote generates membrane vesicles termed heterologous caveolae (h-caveolae; Walser et al., 2012). This suggests a structural role for CAV1 in membrane remodeling, but how the cavins contribute to caveola formation in vivo remains unknown. In cells, cavins exist as large detergent-resistant complexes with sedimentation coefficients between 40S and 60S (Hansen et al., 2013; Hayer et al., 2010). Recent studies have highlighted details of caveola organization including (1) the presence of striations on the surface of caveolae, (2) the ability of cavin1 to form homotrimers, and (3) the existence of at least two distinct cavin subcomplexes incorporating Cavin1-Cavin2 or Cavin1-Cavin3 protein pairs in defined ratios of two to three molecules of Cavin1 per molecule of Cavin2 or Cavin3 (Gambin et al., 2014; Ludwig et al., 2013).

We have identified a universal oligomerization domain, termed the helical region 1 (HR1) domain. The HR1 domain is found in all cavins and promotes specific homo- and heteromeric cavin-cavin interactions, via the formation of a highly extended trimeric coiled coil defined by X-ray crystallographic structure determination. A second helical region (HR2) is formed following initial trimerization, and together these domains are important for the ability of cavins to self-assemble and associate with anionic lipid membranes. Importantly, we find that cavins possess intrinsic

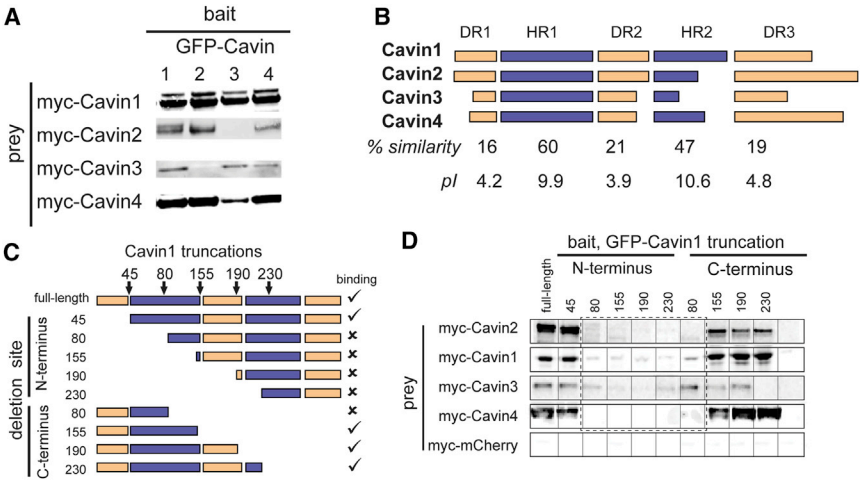

Figure 1. Cavins Possess a Conserved α-Helical Interaction Domain

(A) Pairwise interactions between mouse cavins expressed in the *L. tarentolae* cell free system. GFP-cavin bait proteins were precipitated with GFP-nanotrap beads and bound myc-tagged cavin proteins detected by western blotting. Cavin2 and Cavin3 do not associate with each other.

(B) Schematic representation of disordered and helical domains in mouse cavin sequences. Lengths of bars represent domain relative lengths. Low-homology disordered regions DR1, DR2 and DR3 are drawn in orange, and homologous regions predicted to form α-helical secondary structures HR1 and HR2 are shown in blue. The average similarity and pI values are given under each domain. A full secondary structure-based sequence alignment is shown in Figure S2A. Sites of phosphorylation are shown in Figure S2B.

(C) Schematic representation of Cavin1 truncation library. Arrows indicate truncation positions in respect to HR and DR domains of Cavin1 (as in B).

(D) Pull-downs of myc-tagged full-length prey cavins, mCherry as a negative control, with GFP-tagged truncated forms of Cavin1 as bait. Experiments were conducted and analyzed as in (A). The dashed line highlights pull-downs with Cavin1 baits lacking the HR1 domain that showed little interaction. For original images of individual pull-downs see Figure S1B. For analogous pull-down results for Cavin2, 3, and 4 truncations see Figures S1C–S1E.

membrane remodeling activities that we propose contribute to the mechanism of formation of the caveola membrane invagination. We found that cavins expressed and purified from bacteria subsequently assemble into large lipid-containing particles, and crosslinking and lipid removal reveals the presence of an underlying ordered protein lattice composed of a repeating rod-like element that is strikingly similar to the natural caveolar coat.

RESULTS

Cavins Homo- and Hetero-Oligomerize via a Conserved α-Helical Domain

We first systematically interrogated full-length cavin association using a cell-free expression system (Kovtun et al., 2011; Mureev et al., 2009). *Leishmania tarentolae* is a eukaryotic protozoan organism and the system is able to synthesize full-length cavins (Figure S1A available online). First, we coexpressed pairs of full-length murine cavins and coimmunoprecipitated the resulting complexes using anti-GFP nanobody-coated beads. Probing the pairwise interactions demonstrated that all four cavin species form direct homo- and hetero-oligomers in the absence of other caveolar components. The one exception is that Cavin2 and Cavin3 do not bind to each other, confirming previous observations (Gambin et al., 2014; Ludwig et al., 2013) (Figure 1A).

Next, we sought to define domains required for cavin interactions. To guide our experiments we first performed a combined sequence and secondary structure based alignment of all mouse cavins, and zebrafish Cavin4a (Figure S2A). This identified two regions of strongly predicted α-helical structure that show a high degree of sequence conservation across the family. The first helical region (we term HR1) encompasses a previously predicted coiled-coil domain (McMahon et al., 2009; Parton and del Pozo, 2013). The second helical region (HR2), while also conserved, is less similar among cavins than the HR1 region and is of variable length in different proteins. These domains overlap with "homology regions" identified in previous analyses (Bastiani et al., 2009; Gustincich et al., 1999). The HR1 and HR2 domains are flanked by regions that are poorly conserved and predicted to be disordered which we term DR1, DR2, and DR3. Two observations emerge from these secondary structure-guided alignments. First, the distribution of known phosphorylation sites (Hansen and Nichols, 2010; Yang et al., 2014), primarily map to the DR regions (Figure S2B). Second, the HR1 and HR2 regions show not only high sequence conservation but are also highly basic and positively charged in all species. In contrast, all DRs are acidic and bear a negative net charge (Figure 1B). Thus, all cavins share a common pattern of electrostatically alternating disordered and helical domains along their length.

Based on our analyses, we designed a suite of cavin truncation constructs to assess the role of different cavin domains in homo- and hetero-association. Specifically we analyzed the ability of GFP-tagged cavins with systematically deleted DR and HR domains to bind myc-tagged full-length cavin species (Figures 1C and 1D; Figure S1). These experiments reveal a binding pattern that demonstrates the HR1 domain of all mouse cavin proteins is necessary and sufficient for both homo- and hetero-oligomerization, recapitulating the binding specificities observed for the full-length proteins. As truncations became shorter and approached the boundaries of the HR1 region, we often observed a pattern of weakened association before the interaction was completely abolished. Thus, the HR1 domain acts as a universal oligomerization domain for all cavins, but there may be a small degree of heterogeneity in the domain boundaries. We suggest this is due to the nature of the helical structure of this domain at the N and C-termini (see below).

The Structure of the HR1 Universal Oligomerization Domain of Cavins Reveals a Trimeric Coiled Coil

To gain an insight into the universal mechanism of association between cavins, we determined the X-ray crystal structures of the HR1 domain from mouse Cavin1 (residues 45–155, mC1-HR1) and zebrafish Cavin4a (residues 16–123, zC4-HR1; Figures 2A–2E; Table 1; Figure S3). Both proteins are arranged in highly

similar homotrimeric coiled-coil structures formed by parallel α helices, resulting in rigid cylindrical shaped molecules with a length of ~160 Å and an average diameter of ~26 Å. A pairwise superposition of the mC1-HR1 and zC4-HR1 structures shows that they overlay with a root-mean-square deviation over 279 Cα atoms of 2.2 Å. The similarity of these structures confirms that the HR1 domain of the cavin family forms a trimeric coiled coil that is highly conserved among different cavins and across distant species. The two best structural matches to the HR1 domain as determined using the DALI server (Holm and Rosenström, 2010) were the partial structures of coiled-coil domains from the *Salmonella enterica* trimeric autotransporter adhesin (TAA) SadA (a 40 residue long fragment; Hartmann et al., 2012), and the UspA1 TAA from *Moraxella catarrhalis* (a 138 residue long fragment; Conners et al., 2008). One of the most striking features of the HR1 domain is the presence of a highly basic surface patch (Figure 2D), discussed further below. The homotrimerization of the HR1 domain is also a conserved feature of Cavin2 because mC2-HR1 migrates with a similar elution profile to both mC1-HR1 and zC4-HR1 (Figure 2F).

The majority of residues in both HR1 structures are well ordered, but the C-terminal portion of the mC1-HR1 supercoil cannot be modeled beyond residue Glu146 based on electron density. Overall, the superhelix is stabilized by hydrophobic packing of *a* and *d* residues of a classical coiled-coil heptad repeat sequence (Figure 2E), which is well conserved among the cavins. Cavin3 is a minor exception, as multiple Ala side-chains substitute for bulkier residues present in other cavins within the second half of the HR1 domain (positions 116, 123, 126, and 130 in Cavin1). This may result in decreased stability of the coiled coil in this region, and the stability of Cavin3 could be further compromised by a substitution at the *d*-position of a bulky charged Arg side-chain in place of Gln (Q133 in Cavin1). However, we think these substitutions in the second half of the Cavin3 HR1 domain do not completely prevent homotrimerization for two reasons: first, we find that the mC3-HR1 domain can homo-and hetero-oligomerize in cell-free assays (Figure 1D; Figure S1D), and second a fragment of mC1-HR1 lacking this region altogether (residues 45–103) exists in a stable trimeric form when purified from bacteria (not shown). Like many coiled-coil structures, substitutions at several *a* and *d* positions with polar Gln side-chains are observed in the cavin HR1 domains, providing specificity to the register of the coiled coil. A notable feature of the cavin structures is a conserved His and Thr pair at respective *a* and *d* positions (Gln and Thr in Cavin2), at the center of the HR1 structure (residues His102 and Thr105 in Cavin1). This pair forms a conserved intrachain hydrogen bond that likely provides stability to the structure in this region, and may be required for normal packing and specific interactions of the Cavin coiled coils in this region.

The Cavin HR2 Domain Is α-Helical and Promotes Higher-Order Assembly when Coupled to HR1

Although the HR2 domain is not essential for cavin homo and hetero-interactions, its conservation and high α-helical potential (Figure S2) suggest it will play an important role in the overall cavin structure. The HR2 region is also highly basic, and in Cavin2 has been shown to be functionally required for plasma membrane association (Hansen et al., 2009). Therefore we isolated and characterized the HR2 domains from both mouse Cavin1 (mC1-HR2) and zebrafish Cavin4a (zC4-HR2). Multi-angle-laser light scattering (MALLS) analyses indicate that both are monomeric in isolation (Figure 2G), and in contrast to HR1, circular dichroism (CD) spectroscopy indicated that both HR2 domains are predominantly unfolded in isolation (Figure 2H; only the zebrafish domain is shown).

We next assessed whether the HR2 domain adopts a secondary structure within the full-length protein, using zebrafish Cavin4a (mouse Cavin1 was unsuitable due to instability in the absence of fusion tags). To test this we compared CD spectra of individual HR1 (residues 16-123) and HR2 (residues 151–281) domains to both an HR1-HR2 fragment (residues 16–281) and the full-length protein (Figure 2H), and estimated the percentage of helical structure. The zC4-HR1 domain was almost entirely helical as expected from its crystal structure. Furthermore, both the HR1-HR2 fragment and full-length protein demonstrated very high helical contents (83% and 77%, respectively; Figure 2I). Logically, this is only possible if HR2 adopts a helical structure in the context of full-length protein; if the helical structure is contributed by only the HR1 domain then the total helical contents of the HR1-HR2 fragment or full-length protein would instead be only 46% and 38% respectively. If we instead assume that the HR2 region is 90% helical, then the predicted total helical content would be 82% and 66% for these constructs respectively, in close agreement with the measured values (Figure 2I).

We next investigated whether the induction of secondary structure in the HR2 domain alters the oligomeric state of the Cavin1 complex. For this, we assessed the apparent molecular weights of Ub-tagged full-length, HR1, HR2, and HR1-HR2 fragments of mCavin1 using size-exclusion chromatography (Figure 2J). In agreement with its extended shape, the isolated HR1 domain showed an apparent molecular weight near 120 kDa, and MALLS indicated a molecular weight consistent with a trimeric structure (not shown). The HR2 domain eluted with an apparent molecular weight of ~25 kDa, which is consistent with its lack of secondary structure and its monomeric state as measured by MALLS. However, the Cavin1 HR1-HR2 fragment demonstrated a much higher apparent molecular weight >500 kDa, and the full-length protein eluted with an apparent size in the 1,000–2,000 kDa range, although precise molecular weights could not be estimated by MALLS analysis due to significant heterogeneity of these protein oligomers. These data suggest that cooperative acquisition of helical structure by HR2 in the presence of HR1 results in formation of higher order oligomers beyond the trimeric coiled-coil structure, consistent with previous studies of the full-length proteins in cell extracts.

Cavin HR1 and HR2 Domains Possess Distinct PIP and PS Binding Preferences

The HR1 domain of the cavins possesses a conserved basic surface (Figure 2D). It is known that negatively charged residues of the Cavin2 HR2 domain are important for membrane targeting in cells, but the HR1 domain is also required (Hansen et al., 2009; McMahon et al., 2009). Caveolar membranes are enriched in anionic lipids including the phosphoinositide (PIP) phosphatidylinositol(4,5)bisphosphate (PI(4,5)P_2) (Fujita et al., 2009; Lanzafame et al., 2006) and phosphatidylserine (PS; Zhang et al.,

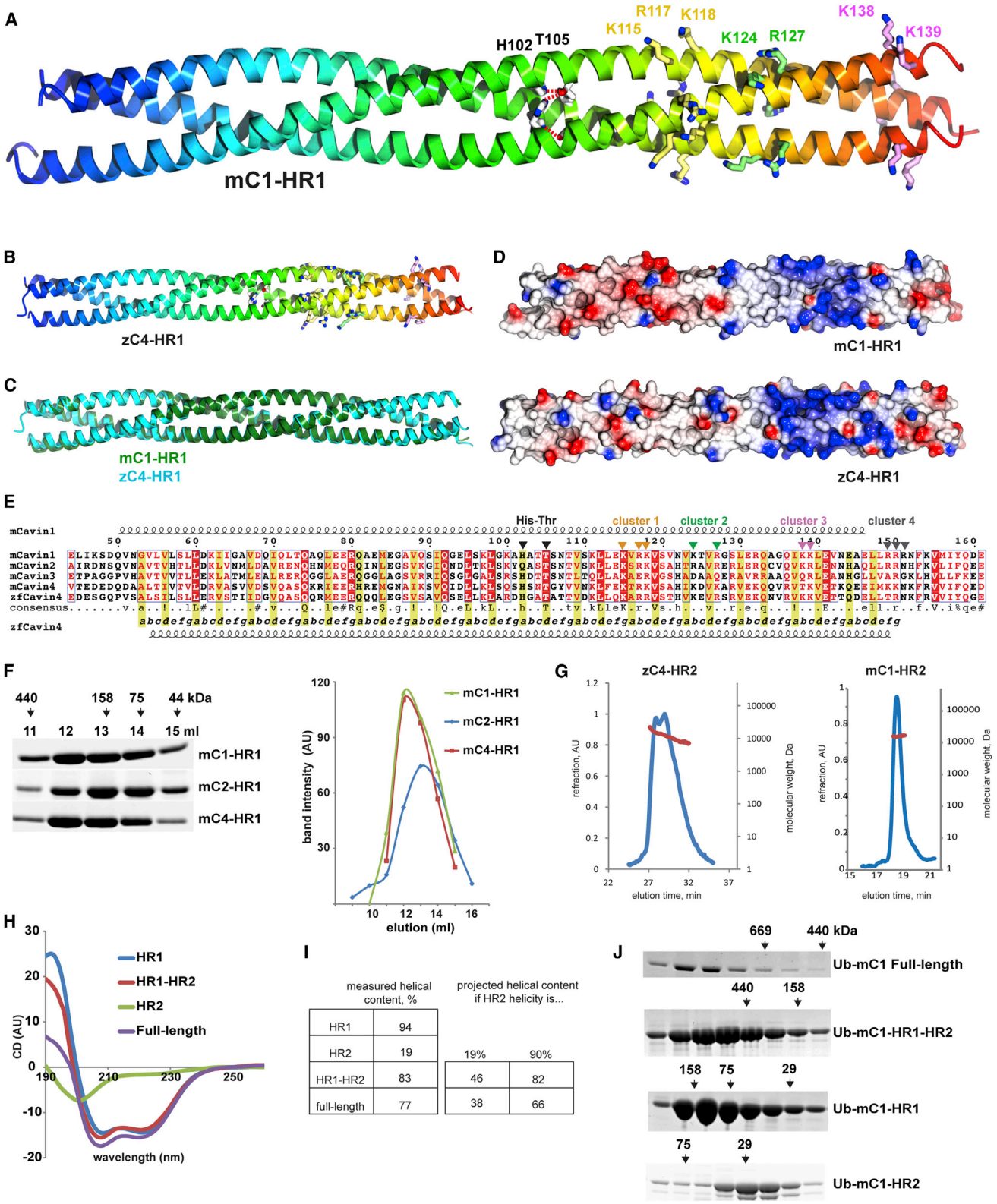

Figure 2. Crystal Structure of the Cavin HR1 Domain and Analysis of Full-Length Proteins

(A) The crystal structure of the mouse cavin HR1 (mC1-HR1) domain reveals a highly extended trimeric coiled coil. The three identical chains are shown as ribbons colored blue to red from N- to C terminus. Also indicated are the side chains of highly conserved structural features; H102 and T105 form a core inter-chain hydrogen bond interaction, and several clusters of basic side chains are present. Electron density and crystal packing is shown in Figure S3.

(legend continued on next page)

2009). The binding of cavins to PS is well documented (Burgener et al., 1990; Gustincich and Schneider, 1993; Hill et al., 2008; Izumi et al., 1997; Mineo et al., 1998) and may be important for the association with caveola membrane domains, whereas the role of PI(4,5)P_2 in cavin sequestration is unknown. The positive electrostatic surface of the cavin HR1 domain is comprised of a number of charged residues located within the C-terminal half that reside in three distinct clusters; cluster 1 (Lys115, Arg117, Lys118), cluster 2 (Lys124, Arg127), and cluster 3 (Lys138, Lys139). A C-terminal cluster 4 is also identified from cavin sequence alignments but is not structurally ordered in either of our crystal structures (Arg149, Arg150, Arg151) (Figures 2A and 2E). The location of these basic residue clusters is highly conserved, and suggestive of additional lipid interaction sites that may explain the dual requirement of both HR1 and HR2 regions for membrane association in cells (Hansen et al., 2009).

We first tested the ability of full-length mouse Cavin1 and Cavin2 to associate with artificial liposomes of defined compositions (Figure 3A). Note that these proteins were first treated with Triton X-100 detergent, to remove *Escherichia coli* lipids that co-fractionate with the full-length cavins (discussed further below). Both proteins showed a high affinity for negatively charged membranes, binding strongly to Folch lipid fractions that are highly enriched in negatively charged lipids, and to membranes containing PS as expected. They also showed a significant interaction with liposomes containing PI(4,5)P_2. Isothermal titration calorimetry (ITC) using Cavin2 showed a significant affinity for PIP headgroups, binding water-soluble PI(4,5)P_2 and PI(3,4,5)P_3 with a K_d between 5 and 30 μM (not shown). This binding affinity is comparable to many other PIP-binding domains studied previously.

Next, we tested a number of constructs including isolated HR1 and HR2 domains, as well as mouse Cavin1 and zebrafish Cavin4 HR1-HR2 constructs lacking the N- and C-terminal disordered regions. Removal of the disordered regions had no effect on membrane binding, indicating that the activity is contained within the structured helical segments (Figure 3B). Interestingly, all HR1 constructs tested from mouse Cavin1, Cavin2, Cavin4 and zebrafish Cavin4a bound robustly to negatively charged Folch liposomes (Figure 3C). However, in contrast to the full-length proteins or the HR1-HR2 fragment, the isolated HR1 domains show a significant preference for PI(4,5)P_2-containing membranes compared to PS. While weak PS binding was observed, after controlling for the total negative charge of the lipids PI(4,5)P_2 was found to bind much more strongly. In addition, membrane buried acidic lipid phosphatidylglycerol (PG) was inefficient compared to PS and PI(4,5)P_2, and the alternative PIP PI(3,4)P_2 showed weaker activity in cavin pelleting assays compared to PI(4,5)P_2 (Figure 3E). This supports the notion that the plasma membrane lipids PS and PI(4,5)P_2 rather than overall negative charge preferentially enhance cavin anchoring to lipid bilayers. Despite the net basic charge caused by an abundance of Lys and Arg residues and previous reports of their significance for membrane association, when we tested binding of the isolated HR2 domains only highly charged Folch liposomes precipitated the domains efficiently (Figure 3D). This suggests that α-helical secondary structure formation and/or oligomerisation driven by the presence of HR1 is important for efficient lipid binding by the HR2 domain. Because the full-length proteins display a uniform ability to bind negatively charged membranes containing either PI(4,5)P_2 or PS, whereas the HR1 domain has a preference for PI(4,5)P_2, we infer that the proteins possess two distinct membrane interaction sites. HR1 mediates stronger interactions with PI(4,5)P_2, and HR2 mediates efficient binding to PS but only in the context of the cavin oligomer driven by coiled-coil formation. Finally, we did not find any evidence for a role of cholesterol in enhancing cavin-membrane association (Figure S4).

We next quantified the interaction of the HR1 domain with soluble lipid headgroups, analyzing zC4-HR1 by ITC (mC1-HR1 was unsuitable for ITC experiments; Figure 3F). The zC4-HR1 protein showed binding to all tested di- and triphosphorylated PIPs, with similar affinities detected for PI(4,5)P_2, PI(3,5)P_2, and PI(3,4,5)P_3, and a slightly lower affinity for PI(3,4)P_2 consistent with the weaker association of cavins with PI(3,4)P_2-containing liposomes (Figure 3E). The heat released on titration of PI3*P*, PI4*P* and PS was indistinguishable from the background. The interaction stoichiometries indicated that each zC4-HR1 trimer contains three independent PIP binding sites. Next we tested if PIP-recognition is mediated by the basic clusters of the HR1 domain. Arg and Lys residues in the basic clusters were substituted with Gln and these mutants were tested in liposome binding assays and ITC with PI(4,5)P_2. These experiments showed that mutations in the first two clusters dramatically

(B) The crystal structure of the zebrafish Cavin4a HR1 domain (zC4-HR1) is shown as for mC1-HR1 in (A).
(C) Structural overlay of the mC1-HR1 (green) and zC4-HR1 (cyan) domains demonstrates their close structural similarity.
(D) Surface representations of mC1-HR1 (top) and zC4-HR1 (bottom) are shown colored for electrostatic potential (red to blue = −0.5 V to +0.5V). The clusters of basic side-chains form a highly positively charged contiguous surface.
(E) Sequence alignment of the HR1 regions of murine cavins and zebrafish Cavin4a. Crystal structure-derived secondary structures for mC1-HR1 and zC4-HR1 are shown at top and bottom, respectively. The conserved His-Thr pair is highlighted, as are the conserved basic side-chain clusters.
(F) Hydrodynamic properties of HR1 domains of mCavin1, 2 and 4 suggest they all form elongated molecules of similar dimensions. Proteins were fractioned on Superdex 200 10/300 column and 1 ml fractions were compared by SDS-PAGE. Arrows indicate molecular weight markers (kDa). Plot at the bottom shows densitometry of bands above.
(G) Estimation of molecular weight of zC4-HR2 and mC1-HR2 domains using MALLS.
(H) CD spectra of constructs of zebrafish Cavin4a.
(I) Experimentally measured helical content of Cavin4a constructs (from H are shown on the left. On the right is the expected helical content of the HR1-HR2 fragment and the full-length protein if (i) the HR2 domain is mostly unstructured (19% helical as measured on its own), or (ii) has a mostly α-helical structure as predicted (90% helical).
(J) The HR2 domain triggers oligomerization resulting in increased cavin mobility by size exclusion chromatography. Ubiquitin-tagged full-length (top) and truncated forms of mCavin1 were fractionated on size-exclusion columns Superose 6 (full length) and Superdex 200 (all truncations) and the fractions were analyzed on PAGE. Arrows indicate elution position and molecular weight of calibration markers.

Table 1. Statistics for X-Ray Crystallographic Structure Determination

	Mouse Cavin1 (45–155); mC1-HR1[a]	Zebrafish Cavin4a (16–123); zC4-HR1
Space group	$P2_12_12_1$	C2
Unit cell dimensions (a, b, c; α, β, γ)	41.0 Å, 98.7 Å, 104.8 Å, 90°, 90°, 90°	114.9 Å, 32.0 Å, 84.8 Å, 90°, 94.5°, 90°
Wavelength	0.97900 Å	0.95370 Å
Resolution range	52.42–3.00 Å (3.16–3.00 Å)	45.8–1.70 Å (1.79–1.70 Å)
I/σ(I)	14.9 (5.4)	13.0 (2.2)
R_{merge}	0.071 (0.295)	0.073 (0.826)
Unique reflections	9,020 (1,293)	211,025 (30,445)
Multiplicity	8.3 (8.6)	6.1 (6.2)
Completeness	99.7% (99.9%)	100.0% (100.0%)
Anomalous multiplicity	4.5 (4.6)	–
Anomalous completeness	99.7 (100.0)	–
MR-SAD Phasing		
Figure of merit	0.728	–
Number of Se sites	8	–
Bayes-CC	75.5	–
Map skew	1.57	–
Correlation of local RMS density	0.92	–
Refinement		
Resolution range	37.89–3.00 Å (3.19–3.00 Å)	42.5–1.70 Å (1.75–1.70 Å)
No. reflections/ no. R_{free}	8,944 (1,306)/ 889 (150)	34,226 (2,659)/ 1,731 (141)
R_{work}/R_{free}	0.224 (0.262)/ 0.283 (0.329)	0.214 (0.272)/ 0.245 (0.312)
Protein chains (modeled residues)	A (46–146); B (52–144); C (53–143)	A (18–118); B (20–118); C (20–116)
Number of Atoms		
Protein	2,162	2,531
Solvent	13	238
Average *B*-factor	92.5 Å^2	35.8 Å^2
Root-Mean-Square Deviations		
Bond lengths	0.009 Å	0.006 Å
Bond angles	1.28°	0.83°

[a]Values in parentheses are for the highest-resolution shell.

decreased lipid binding of zC4-HR1 with no binding detected by ITC if both cluster 1 and 2 are mutated together (5Q mutant), (Figure 3G). All mutants retained proper helical structure (not shown). A similar reduced binding profile was seen for mC1-HR1 mutants by liposome pelleting (Figure 3H). Lastly, we tested the importance of the HR1 basic clusters 1 and 2 (5Q mutant) in the context of the full-length mouse Cavin1 protein and the zebrafish Cavin4a HR1-HR2 construct (Figure 3I). Mutation of HR1 in proteins including the HR2 domain reduced PI(4,5)P_2 binding, although it did not abolish it completely, while it had little effect on PS interaction. Again, this argues for a distinct site within the HR1 domain that preferentially governs PIP association.

The Cavins Possess Intrinsic Membrane Remodeling Properties In Vitro

Cavin proteins are essential for the normal formation and morphology of caveolae (Bastiani et al., 2009; Hansen et al., 2009; Hill et al., 2008; Liu et al., 2008), and Cavin2 has been shown to generate membrane tubules when overexpressed (Hansen et al., 2009). However, whether the cavins have an ability to promote membrane remodeling or membrane invagination in the absence of other cellular components is unclear. First, we examined the isolated cavin HR1 domain by incubation with artificial liposomes. Using EM, we observed a striking effect of zC4-HR1 on PI(4,5)P_2/PS-containing liposomes causing strong accumulation of deformed and compacted membrane material (Figure 4A). Ub-mC1-HR1 modified liposomes in the same way (not shown). Liposome agglutination was detectable both with EM and turbidity measurements of liposomes in solution (not shown), and suggests the presence of multiple lipid-binding sites on the surface of the HR1 domain. Liposome agglutination was dependent on anionic lipids, because no effect on neutral PC/PE liposomes was observed. Concomitantly, ablation of the PIP-binding site in the zC4-HR1 5Q mutant nullified the ability to agglutinate and compact lipid membranes.

When the same assays are conducted using full-length mouse Cavin1 and Cavin2 proteins, we observe a striking ability to remodel PI(4,5)P_2/PS liposomes (Figures 4B and 4C respectively). Both proteins promote the formation of long membrane tubules with a median (but relatively heterogeneous) diameter of approximately 60 nm (Figure 4D). Liposome tubulation was triggered at relatively low protein concentrations (~1–3 μM), suggesting a significant propensity for membrane remodeling by cavins. As low as 1:300 protein:lipid molar ratio was sufficient to observe tubulation by Cavin2 of the classical liposome substrate composed of Folch brain extract, while Cavin1 caused tubulation at a 1:100 ratio (Figure S5). Unlike the HR1 domain, full-length cavins did not cause liposome agglutination. Apart from tubule formation, Cavin1 also triggers the consistent formation of small buds connected through a common stem (Figure 4B). These data suggest that both HR1 and HR2 domains are required for normal association of cavins with lipid membranes, and cavins can induce or stabilize membrane curvature even in the absence of other cellular components.

The PIP-Binding Site of Cavin1 Promotes Caveola Localization

To investigate the physiological role of the PIP-binding site, we studied localization of the mutant Cavin1 protein in a specific cell model. To avoid interference from other cavins, we used the human prostate cancer cell-line PC3 deficient in all four cavins (Bastiani et al., 2009). The plasma membrane of these cells contains no morphological caveolae. Previous work demonstrated that GFP-Cavin1 re-expression is sufficient to restore caveola formation and decrease caveolin mobility in these cells and GFP-Cavin1 and CAV1 colocalize in plasmalemmal puncta when observed by fluorescent microscopy (Bastiani et al., 2009; Hill et al., 2008). Therefore, we transiently expressed GFP-Cavin1 wild-type and 5Q mutant proteins and studied their

cellular localization. Because a high level of expression resulted in diffuse distribution for both proteins, we excluded cells showing high GFP brightness. As expected, heterologously expressed wild-type GFP-Cavin1 localized primarily in CAV1-positive puncta. However, the 5Q mutant yielded a significantly lower fraction of cells showing punctate localization (Figures 5A–5C). Notably, cells expressing mutant GFP-Cavin1 5Q did occasionally show puncta of GFP fluorescence. Consistent with cell localization data, we observed a small but significant increase in the cytosolic pool of the 5Q mutants compared to the WT proteins using sedimentation assay (Figure 5D), suggesting that the loss of the PIP-binding site perturbs but does not abolish the association with cell membranes. In addition, the 5Q mutation does not alter the morphology of caveolae that can be seen by electron microscopy (Figure S6). The relatively mild phenotype of the 5Q mutant correlates with its lipid interaction properties in vitro. The 5Q mutation in the full-length mCavin1 or zCavin4 (HR1-HR2) fragment while decreasing their affinity for PI(4,5)P_2-containing liposomes, had little effect on binding to PS liposomes (Figure 3I), and was also capable of tubulating liposomes similarly to the wild-type protein (not shown). We conclude that PIP-interaction with the HR1 domain can enhance membrane association but is not strictly required for caveolar formation. Finally, we wished to examine whether the HR1 domain is alone sufficient for caveola recruitment so GFP-mC1-HR1 was expressed in PC3 cells and compared with GFP alone (Figure 5E). This construct showed a cytoplasmic distribution very similar to GFP protein alone, and no observable localization to CAV1-positive structures; therefore, we conclude that other Cavin1 domains are additionally required to mediate caveolar recruitment.

Cavins Self-Assemble into Lipid-Containing Protein Particles in *E. coli*

With systems established for purifying recombinant cavin proteins, we next characterized the architecture of the homo-oligomeric complexes formed by full-length proteins. Mouse Cavin1, expressed in *E. coli*, yielded large assemblies that migrate in the excluded volume of a Superose 6 size exclusion column (Figure S7). Using negative staining EM the purified complex appears as spherical hollow particles with a relatively narrow size distribution and average diameter of 22.3 ± 4.9 nm (n = 330; Figures 6A and 6B). Expression of mouse Cavin2 and zebrafish Cavin4a lead to formation of similar particles, although with slightly differing average sizes (Figures 6A and 6B). Studies using Cryo TEM of Cavin1 particles confirmed the generally spherical shape, and showed that the walls have an apparent thickness of 5.3 ± 0.9 nm (Figure 6C). While this thickness resembles that of a lipid bilayer (~5 nm), unlike a bilayer the particle walls have a highly heterogeneous electron density. In addition, lipid bilayers in vesicles of this narrow diameter would be extremely rigid due to the high curvature, and would be expected to form a nearly ideal spherical shape. In contrast, Cavin1 complexes noticeably deviate from an ideal sphere with uneven densities observed.

Because cavins are potent binders of lipid membranes, we tested isolated Cavin1 complexes for the presence of lipids using thin-layer chromatography. These assays indicate that isolated Cavin1 particles do contain significant amounts of lipid, extracted from *E. coli* membranes during protein purification (Figure S7A). As lipids can reduce contrast in EM, we removed them from the Cavin1 complex using Triton X-100 detergent. Detergent-treated Cavin1 samples were freed from lipids as measured by thin-layer chromatography, and the treatment also caused a significant change in hydrodynamic radius of the complex as assessed qualitatively by size exclusion chromatography (Figures S7A and S7B). Although smaller than the lipid-containing assemblies, the detergent treated complex still retains an apparent size above 1 MDa; however, negative stain EM of these samples no longer showed morphologically distinct particles (Figure S7C). Intensive crosslinking with amino reactive glutaraldehyde confers detergent resistance to the lipid-containing cavin particles (Figure S7C).

Cavins Form Rod-like Structures that Organize into Larger Assemblies via Lateral Interactions

To discern the ultrastructure of the underlying Cavin1 protein assemblies, we tested a variety of conditions for milder crosslinking and detergent treatments that would increase contrast in EM imaging but not disassemble the cavin structure completely. We found that a combination of paraformaldehyde crosslinking followed by Triton X-100 treatment of Cavin1 particles on EM grids results in the striking appearance of rod-like structures arranged in regular arrays, with a uniform spacing between the rod-like elements (Figures 6D and 6E). The dimensions of these rods were relatively consistent and measured 23.4 ± 3.2 nm in length and 5.5 ± 1.4 nm in width, with a periodic spacing of ~7 nm (Figures 6F–6H). The rods can apparently form oligomers through extensive lateral interactions, with evidence for end-to-end association apparent as well. We suggest these linear assemblies contribute to the "walls" of the intact cavin lipid-containing protein particles, and likely represent the structural building blocks of the striations characteristic of native caveolae.

DISCUSSION

We report the structure of the HR1 core oligomerization domain found in all cavins. This domain forms a structurally conserved trimeric coiled coil, which we propose dictates the underlying stoichiometry and composition of cavin complexes. It has been shown that when Cavin1 homo-oligomerizes with Cavin2 or Cavin3 it does so in a ratio between 2 and 3:1 (Gambin et al., 2014; Ludwig et al., 2013), and Cavin2 and Cavin3 cannot associate with each other independently (Figure 1A; Gambin et al., 2014; Ludwig et al., 2013). The trimeric structure of the HR1 assembly domain provides a potential explanation for these findings. First, the subunit ratios of Cavin1:Cavin2 and Cavin1:Cavin3 assemblies imply that only one molecule of Cavin2 or Cavin3 can be accommodated within a heterotrimeric coiled-coil structure. This is likely due to distinct packing geometries of the residues in the *a* and *d* positions of the heptad repeats for the different cavins, as well as the potential for surface associated salt bridges to form between the heteromeric pairs, as this has been shown to be important for specificity in other coiled-coil structures (Ciani et al., 2010; Steinmetz et al., 2007). Similar considerations may also explain the inability of Cavin2 and Cavin3 to associate with each other. The precise residues that dictate these

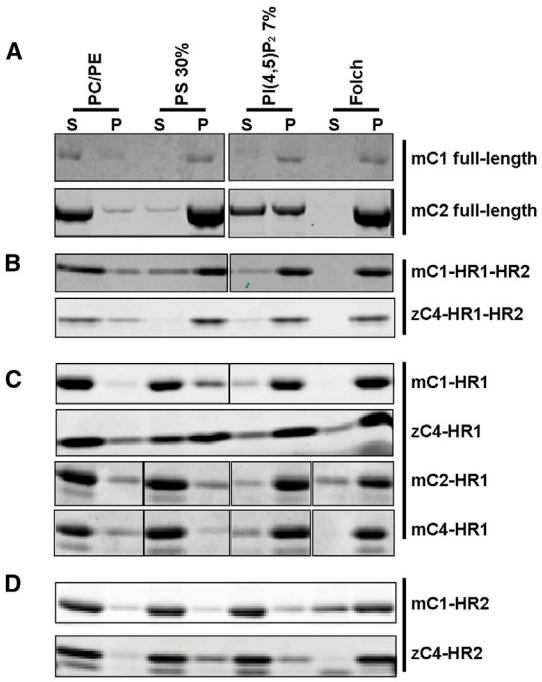

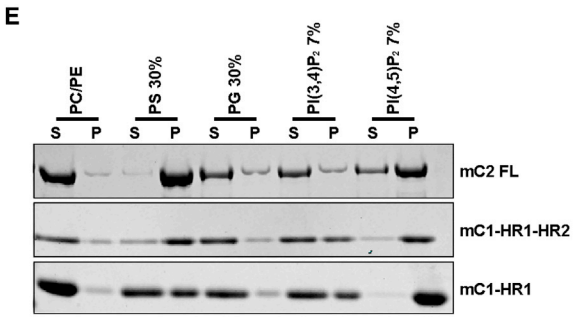

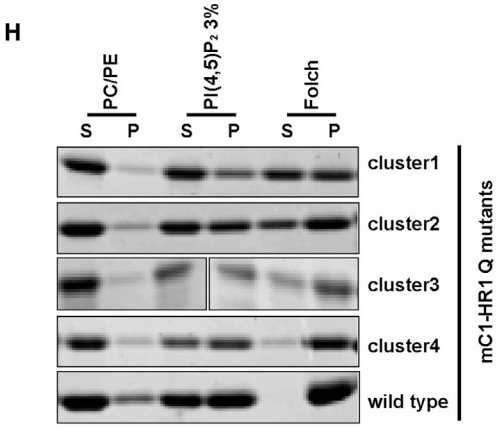

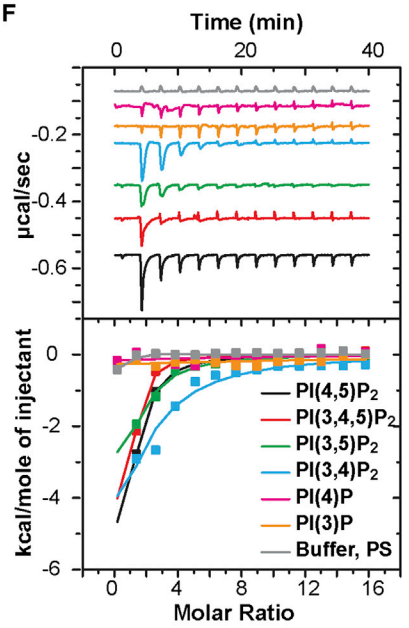

Lipid	Kd, µM	Ratio, N
PI(4,5)P_2	4.5 ± 1.3	1 ± 0.2
PI(3,4,5)P_3	1.9 ± 0.9	0.8 ± 0.1
PI(3,5)P_2	7.5 ± 1.4	1.2 ± 0.1
PI(3,4)P_2	21.6	1.1
PI(4)P	na	na
PI(3)P	na	na
PS	na	na

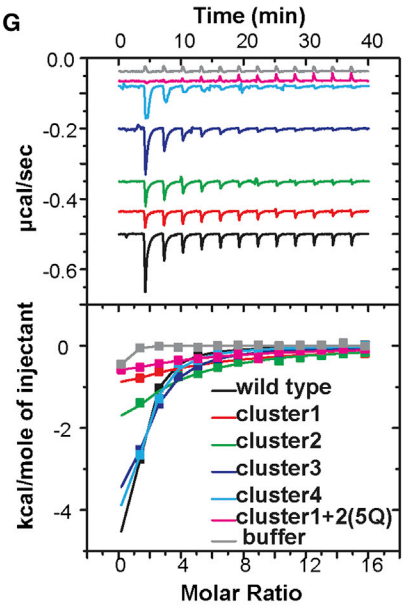

Mutant	Kd, µM
cluster1	68.9 ±1.3
cluster2	40.5 ± 0.6
cluster3	9.0
cluster4	5.5
cluster1+2 (5Q)	na
wild type	4.5 ± 1.3

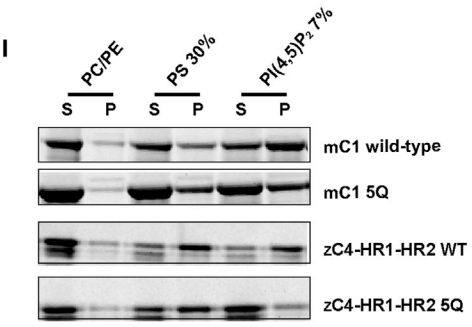

(legend on next page)

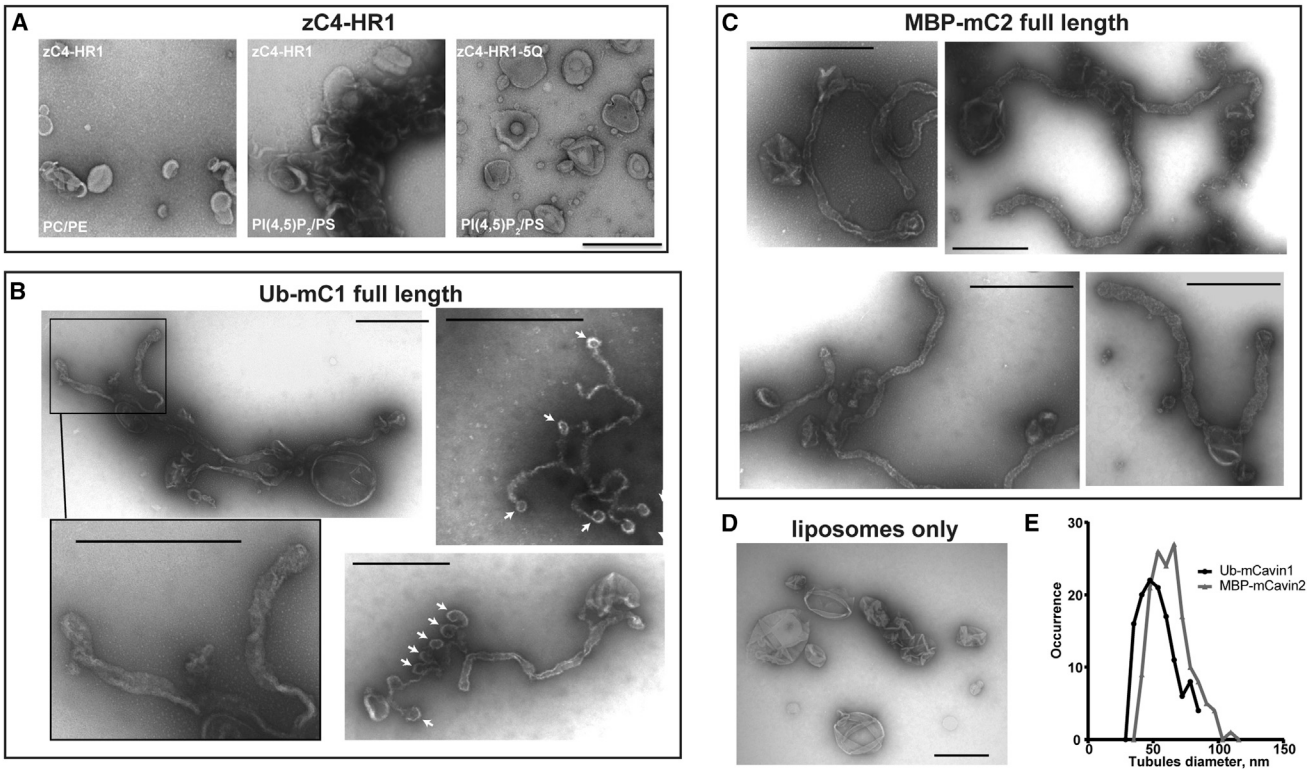

Figure 4. The Cavins Possess Intrinsic Membrane Remodeling Activity

(A) As seen by electron microscopy of UA negatively stained samples, the HR1 domain of zebrafish Cavin4 shows a strong propensity for membrane agglutination, causing the accumulation of PI(4,5)P_2-containing liposomes. Mutation of the basic residues making the strongest contribution to PIP interactions (mC1-HR1-5Q) inhibits this activity.

(B and C) Full-length mouse Cavin1 (B) and Cavin2 (C) proteins are able to cause tubulation of liposomes containing PS and PI(4,5)P_2. Arrows in (B) point at characteristic vesicles generated only upon Cavin1 addition. Electron micrographs show liposomes following protein incubation and after glutaraldehyde/OsO_4 fixation and UA staining. All scale bars represent 500 nm.

(D) Negative control liposomes, untreated.

(E) Quantitation of tubule diameters from (B) and (C).

specificities remain unknown, however, and will require studies of mixed assemblies. A notable feature of the cavin HR1 domain is a stabilizing intersubunit hydrogen bond between conserved His and Thr side-chains (His102, Thr105 in mouse Cavin1) lying at respective *a* and *d* positions in the center of the domain. Interestingly, phosphorylation of this strictly conserved Thr side-chain (and neighboring Ser in Cavin1 and Cavin3) has been reported following insulin stimulation, although its importance remains unknown (Humphrey et al., 2013).

In addition to its role in protein oligomerization, the cavin HR1 domain has a conserved anionic membrane-binding surface. Mutation of this site perturbed the ability of Cavin1 to associate with membranes in vitro and caveolae in cells, although it did not abolish caveola formation completely. This is likely due to the presence of additional cavin domains that contribute to stabilizing Cavin1 interactions with caveolae, including additional clusters of basic side chains in HR1 and the C-terminal HR2 domain. The cavins also possess an intrinsic ability to contribute to the reshaping and sculpting of membranes, consistent with generation of lipid tubules by Cavin2 when overexpressed (Hansen et al., 2009). The mechanism by which cavins promote membrane tubulation is still unclear, but likely involves oligomerization of the cavins into polymeric structures that may be stabilized by interaction with the membrane itself.

Figure 3. Cavins Interact with Membranes

(A–D) Various cavins and cavin domains were profiled for binding to lipid membranes using liposome-pelleting assays. The content of specific anionic lipids is indicated above. S indicates supernatant (unbound), P indicates liposome pellet (bound) protein fractions.

(E) Pelleting assay comparing cavin-binding efficiency of equally charged liposomes containing various acidic lipids: PS, PI(4,5)P_2, PG and PI(3,4)P_2.

(F) Direct association between PIP headgroups and zebrafish Cavin4a HR1 domain (zC4-HR1) measured by ITC.

(G) The role of individual basic clusters of the zC4-HR1 domain in PI(4,5)P_2 binding were tested by mutagenesis. Clusters as indicated in Figure 2E were mutated to Gln.

(H) Similar mutations were introduced into the mC1-HR1 domain and tested in liposome pelleting assays revealing a similar requirement for cluster 1 and cluster 2 for proper membrane association.

(I) Comparison of in vitro lipid-binding of 5Q (cluster1+cluster2) mutant and WT forms of mCavin1 and zCavin4. Experiment was conducted as in (A)–(D).

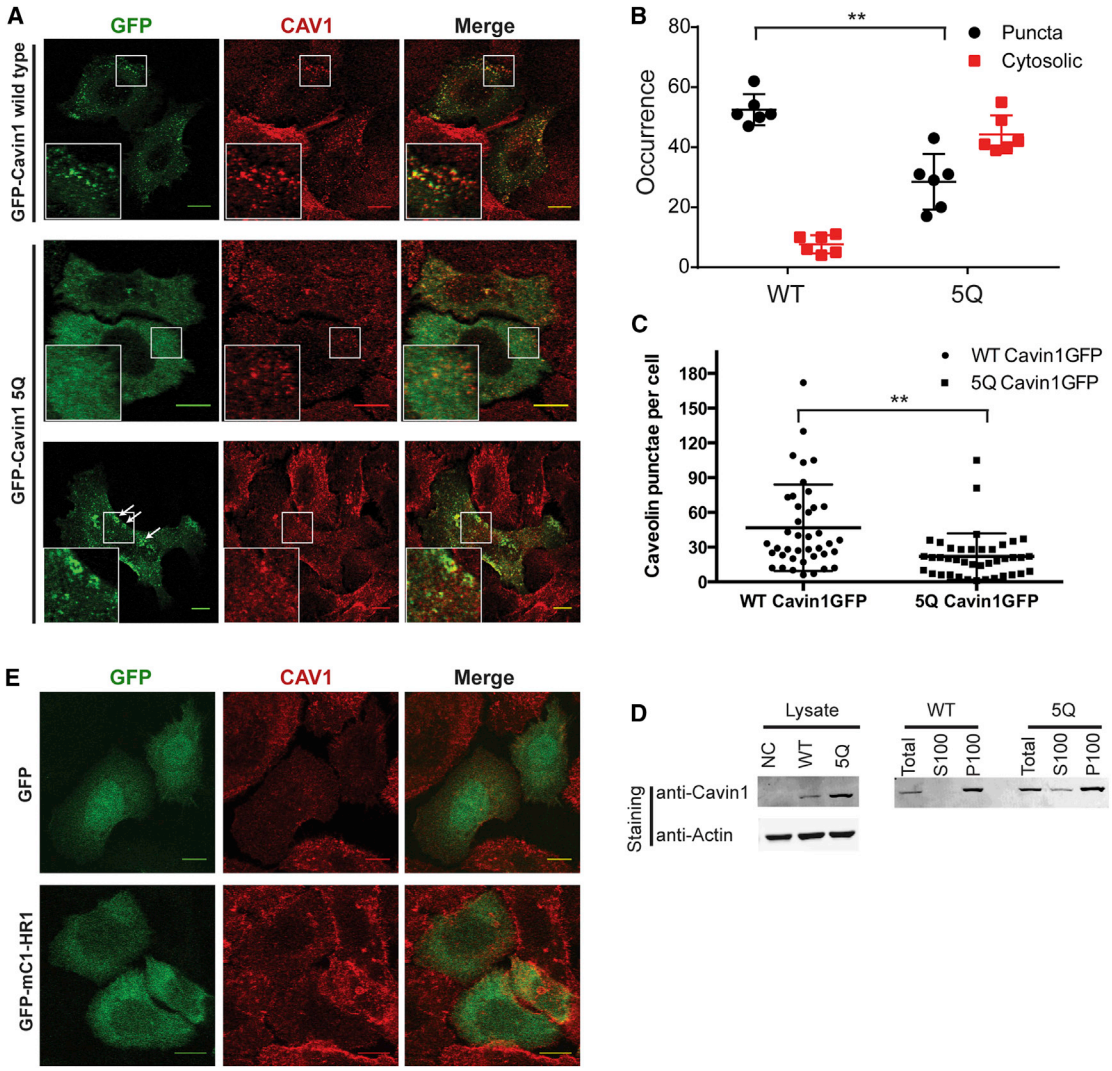

Figure 5. Binding of the HR1 Domain to Membranes Is Important but Not Essential for Caveolar Recruitment

(A) Fluorescent microscopy of PC3 cells transfected with GFP-tagged wild-type (upper row) or 5Q mutant, (middle and bottom rows) of mouse Cavin1. Fixed cells were also stained for CAV1. Wild-type (WT) protein showed a prevailing punctate distribution of GFP fluorescence colocalizing with CAV1, while most cells transfected with mutant protein had a diffuse distribution. Cavin1-5Q transfected cells often contained larger Cavin1 structures (white arrows), and did colocalize with CAV1 in a sub-population of cells. Scale bar represents 10 μm.

(B) Quantitation of the number of cells showing either punctate or cytosolic distribution of WT/5Q Cavin1. Each data point represents a separate biological repetition of the experiment (6 in total), and the total number of analyzed cells was 367 and 437 for WT and 5Q respectively. **$p < 0.05$ (Mann-Whitney test).

(C) Quantitation of the number of puncta per cell in cells expressing either WT or 5Q Cavin1. **$p < 0.05$ (Mann-Whitney test).

(D) Comparison of fractionations of free and membrane bound Cavin1 by sedimentation of cell lysates from transiently transfected cells. S100 and P100 represent supernatant (free) and pelleted (membrane-bound) protein pools. Only the 5Q mutant shows significant membrane dissociation.

(E) GFP-mC1-HR1 was expressed in PC3 cells and compared with GFP alone. The Cavin1 HR1 domain does not localize to caveolae in the absence of other domains. Scale bar represent 10 μm.

Full-length cavins assemble into large multimeric complexes upon heterologous expression in bacteria demonstrating an inherent propensity for self-assembly, also observed in vivo (Gambin et al., 2014; Hayer et al., 2010; Ludwig et al., 2013). Crosslinking prior to lipid removal reveals the presence of a basic building block of these cavin complexes—a rod measuring ~24 nm long and ~5.5 nm wide. The HR1 domain, the only resolved structural element of the cavins, spans over 16 nm and has a diameter of 2.5 nm. The cavin rod-like elements have a diameter that is only slightly wider than that of the rigid cavin HR1 coiled coil but is approximately 10–12 nm longer. In addition to the HR1 coiled-coil domain, the HR2 domain of the full-length Cavin1 is also expected to be α helical in structure (involving ~50–70 residues as estimated by secondary structure prediction), and this is experimentally supported by analyses of the zebrafish Cavin4a protein (Figures 2G and 2H). Our assumption is that the extended density of the rod element structures observed by EM is composed primarily of the HR2 domain

(Figure 6G). The uniform density of the cavin rod-elements suggests they are likely composed of a single cavin trimer. However, we cannot exclude that the 5 nm width observed by negative-stain EM potentially accommodates more than a single 2.5 nm wide trimeric coiled coil.

These rods appear to form ordered arrays via lateral and end-to-end contacts, and remarkably, laterally packed rods demonstrate a characteristic periodic spacing of ~8 nm, similar to the previously identified spacing of cavin densities in the native caveolar coat using miniSOG labeling (Ludwig et al., 2013). We propose that each rod element is composed of either a cavin trimer (or potentially a bundle parallel cavin trimers), and that the inter-rod interactions reflect the organization of cavins within the native caveolar coat. Deep-etch EM methods also identified distinctive striations with similar dimensions and arrangements to our cavin rod elements on the surface of caveolae (Fernandez et al., 2002; Rothberg et al., 1992). Supporting previous speculation (Ludwig et al., 2013), our data indicate that it is the peripheral membrane cavin proteins that generate these distinct membrane coat structures.

Combining our results with previous studies, we propose the following model of caveola assembly. First cavins trimerize via formation of the coiled-coil structure in their HR1 domains (Figures 7.1 and 7.2). Formation of homomeric and heteromeric complexes of Cavin1-Cavin2 or Cavin1-Cavin3 (Gambin et al., 2014; Ludwig et al., 2013) is likely to be controlled by monomer availability. This suggests the primary mechanism for regulating the composition of cavin assemblies will be by different expression profiles in various tissues (Hansen et al., 2013). The architecture of the HR1 trimerization domain controls cavin stoichiometry, allowing a single Cavin2 or Cavin3 molecule per two Cavin1 monomers (Figure 7.2). Trimerization promotes α-helical secondary structure formation in the HR2 domain, resulting in formation of the underlying rod-like structural unit of the caveolar coat (Figure 7.3). These rods associate further into soluble cavin oligomers (Figure 7.4). While we find that cavin proteins expressed in bacteria assemble into large assemblies that copurify with a significant fraction of bound lipids, whether the cytoplasmic cavin oligomers observed in vivo also contain lipids is unknown. Based on the size of an average Cavin1 lipid-containing particle these complexes could accommodate up to 17 cavin rods, totalling >50 monomers per subcomplex. This estimation correlates well with previous reports of cavin proteins expressed in mammalian cells (Gambin et al., 2014; Hayer et al., 2010). Cavins display a relatively high affinity for membranes containing PI(4,5)P_2 (and other PIPs) and PS, and possess inherent anionic lipid-dependent membrane remodeling properties in vitro. These lipids have been found to be present within caveolae, with PI(4,5)P_2 being concentrated around the neck (Fujita et al., 2009; Lanzafame et al., 2006; Zhang et al., 2009). In cells cavins are likely to be dynamically distributed between cytosolic and membrane fractions in the absence of caveolin (Hansen et al., 2009; Figure 7.5). In the presence of caveolin however, cavins stably associate with caveolar membrane invaginations, using coincident PIP and PS binding sites. Increased density of cavins may then allow formation of organized protein arrays that subsequently promote membrane remodeling and formation of characteristic caveolar pits (Figure 7.6). While it is speculative, we believe the alternating electrostatic profile of the cavins may be essential to the formation of these protein arrays. The precise mechanism by which caveolin and cavins cooperate to form the bulb-like structure is unknown. But given the inherent ability of caveolins to generate caveola-like structures in a model system (Walser et al., 2012), it almost certainly requires the associated oligomerization of caveolins, may involve cavin-caveolin protein-protein interactions (Bastiani et al., 2009), and also requires the presence of cholesterol (Breen et al., 2012; Hailstones et al., 1998; Rothberg et al., 1992; Westermann et al., 2005). Notably, cavin excess leads to elongated caveolae or long membrane tubules (Hansen et al., 2009). The mechanism of caveola disassembly is less clear, but it is known that membrane stretch is able to drive dissociation of cavins (Gambin et al., 2014; Sinha et al., 2011; Figure 7.7). Cavins are also known to be highly phosphorylated (Figure S2B), for example following insulin receptor stimulation (Humphrey et al., 2013), and we suggest this could be an additional mechanism for cellular regulation of caveola formation.

In summary, the work presented here provides a glimpse into the mechanism of caveola coat formation at the molecular level and provides a platform for further atomic level studies of these enigmatic membrane structures.

EXPERIMENTAL PROCEDURES

Supplemental Experimental Procedures provide more detailed methods, as well as the specifics of recombinant protein handling, cell culture, biochemical analysis, and immunofluorescence microscopy, including the expression vectors, lipids, and antibodies used in these experiments. Raw diffraction data are available on the DIMER webserver (https://dimer.uq.edu.au).

Protein Crystallization and X-Ray Crystallographic Structure Determination

Mouse Cavin1 and zebrafish Cavin4a HR1 domains were crystallized by sitting drop vapor diffusion at 25°C. The mC1-HR1 domain was solved by a combination of molecular replacement and single wavelength anomalous dispersion (MR-SAD). Initial MR was performed using PHASER with a fragment of the coiled-coil domain of the SadA protein (Hartmann et al., 2009). The MR solution was then used to perform selenomethionine MR-SAD using AutoSol in the PHENIX suite. The structure was subject to multiple rounds of refinement in PHENIX.REFINE and rebuilding in COOT. The structure of the zC4-HR1 domain was subsequently determined by molecular replacement using PHASER. Data and refinement statistics are given in Table 1.

CD Spectroscopy and MALLS

All CD measurements were performed using 20 μM proteins in GF150 buffer using a 0.1 mm path-length cuvette at 25°C. Size exclusion chromatography MALLS was conducted as described previously (Folta-Stogniew and Williams, 1999).

Liposome Preparation and Pelleting Assay

Liposomes were prepared as described elsewhere (Murray and Tamm, 2009). The typical base composition was POPC:POPE (70%:30%), supplemented with different PIPs and acidic phospholipids (PS and PG) at the indicated concentrations. For Folch liposomes, Folch fraction I (Sigma) was used at 100%. For pelleting assays protein and liposomes were incubated in a total volume of 100 μl at 5 μM and 0.5 mg/ml respectively for 10 min at 25°C and liposomes collected by centrifugation at 60,000 × *g* for 10 min at 22°C in TLA100 rotor.

Isothermal Titration Calorimetry

Measurements were performed in GF150 buffer. Water-soluble lipids at concentrations of 500 μM were titrated into 200 μl of 20 μM of protein in a series of 12 injections of 3.22 μl each at 25°C using a MicroCal ITC200 system (GE Healthcare). Dissociation constants and stoichiometries were obtained in ORIGIN using a single sites binding model.

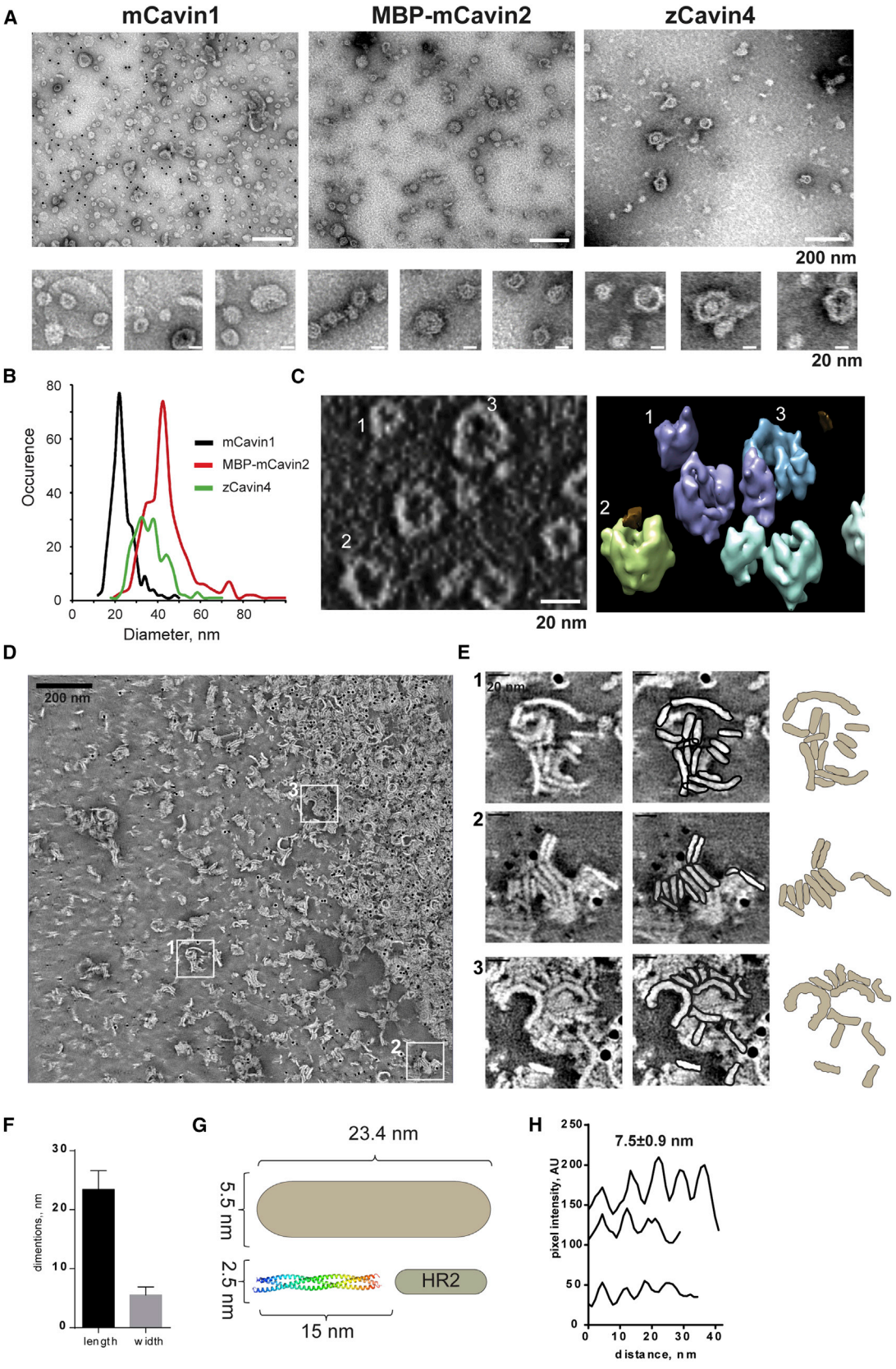

(legend on next page)

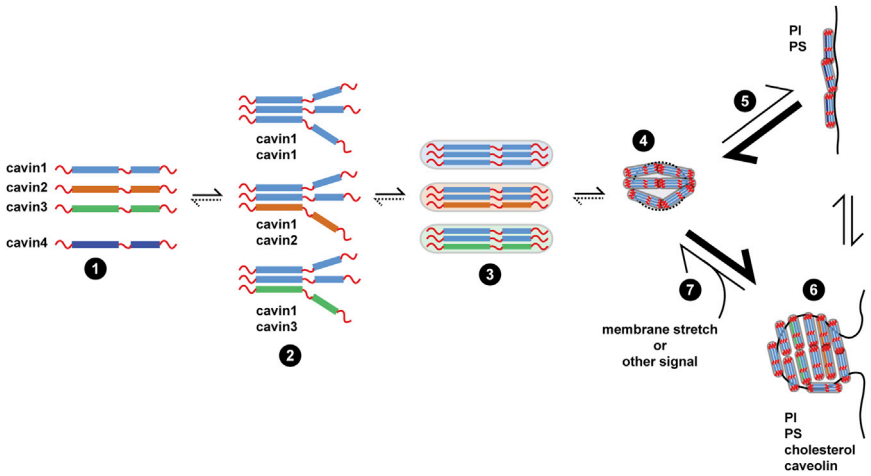

Figure 7. Model for the Assembly of the Cavin Coat

(1) Individual cavin subunits are likely unstable in isolation. (2) HR1 trimerization initiates assembly. In hetero-oligomers, two Cavin1 subunits can bind either a single Cavin2 or Cavin3 subunit. Cavin2 and Cavin3 cannot interact with each other. Stoichiometries of Cavin4 hetero-oligomers have not been studied. (3) HR2 folds into a helical structure and cavin rods can be formed. (4) Cavin oligomeric particles can assemble. These may have lipids present, and could represent the stable complexes generated upon caveola disassembly in cells. (5) Cavin assemblies can associate with PS and PIP-containing membranes. (6) However, cavins are only stably associated with caveolae in conjunction with caveolin (and possibly cholesterol). Cavin striations are formed through lateral and end-to-end contacts, and these interactions may be dependent on the attractive electrostatic potentials of the HR and DR regions. Cavin2 and Cavin3 are observed in distinct striations on the surface. (7) Cavins can be dissociated by membrane stretch.

Electron Microscopy Imaging and Data Processing

Cavin lipid-containing protein particles (MBP-mCavin2, untagged zCavin4, and 6his-mCavin1) were absorbed onto glow-discharged carbon coated formvar grids and stained with 1% uranyl acetate (UA) solution. For imaging of de-lipidated cavin complexes, protein was adsorbed on poly-L-lysine coated formvar grids. After washing, material was crosslinked with 4% paraformaldehyde for 10 min and then lipids were washed off the adsorbed material by 10 min incubation in buffer containing 0.05% of TX-100. Sample was further contrasted by 1% UA. For cryo-electron microscopy of Cavin lipid-containing protein particles, protein samples were transferred onto a C-flat holey carbon grid, in an FEI Vitrobot Mark 3, with the chamber set to 4°C and 100% humidity, and plunged into liquid ethane. Observation of caveolae in PC3 cells was performed as described previously (Hill et al., 2008).

Liposome Tubulation Assay

Liposomes at 0.1–0.5 mg/ml were mixed with 1.0–12.5 μM protein in GF150 buffer with 1 mM TCEP and incubated for 10 min at 25°C. Reaction mixtures were then applied to formvar carbon-coated glow-discharged grids for 40 s, and stained by 1% uranyl acetate. In Figures 4B–4D, we used an additional glutaraldehyde/osmium 15 min fixation to preserve membrane tubules intact as described previously (Matsuoka and Schekman, 2000).

ACCESSION NUMBERS

The Protein Data Bank accession numbers for the coordinates and structure factors for the mouse cavin1 HR1 domain and zebrafish cavin4a HR1 domain reported in this work are 4QKV and 4QKW.

SUPPLEMENTAL INFORMATION

Supplemental Information includes Supplemental Experimental Procedures, seven figures, and two movies and can be found with this article online at http://dx.doi.org/10.1016/j.devcel.2014.10.002.

AUTHOR CONTRIBUTIONS

O.K. and V.A.T. determined crystal structures with assistance from B.M.C and S.J.H. O.K. and V.A.T. performed all lipid-binding experiments. O.K. performed the molecular EM studies with assistance from N.A., G.P.M., and C.F. V.A.T., C.F., and R.G.P. performed cellular EM studies. O.K., V.A.T., and N.L. performed protein purification and cloning. W.A.J. produced cell free lysates, and R.A.M. initiated in vitro interaction assays subsequently completed by W.J. and O.K. V.A.T. performed cellular studies, assisted by N.C. K.A., R.G.P., and B.M.C. conceived and initiated the study. O.K., V.A.T., R.G.P., and B.M.C. wrote the paper.

ACKNOWLEDGMENTS

The authors acknowledge support from the staff and facilities of the University of Queensland Remote Operation Crystallisation and X-ray facility, and the Australian Synchrotron. Confocal microscopy was performed at the Australian Cancer Research Foundation (ACRF)/Institute for Molecular Bioscience Dynamic Imaging Facility for Cancer Biology, established with funding from the ACRF. The authors acknowledge the facilities, and the scientific and technical assistance, of the Australian Microscopy & Microanalysis Research Facility at the Centre for Microscopy and Microanalysis, The University of Queensland.

Figure 6. Cavins Form Large Lipid-Containing Assemblies when Expressed in Bacteria that Possess a Core Rod-like Structural Element

(A) Negative stain EM of particles isolated from *E. coli* expressing various full-length cavins. Panels under each image show magnified regions of the same sample grid. These particles contain some bound lipids as shown biochemically in Figure S7.
(B) Size distribution of cavin lipid-containing protein particles estimated from negative stain EM microscopy.
(C) Cryo TEM tomography of mCavin1 complexes. Left: a single plane of tomography density map; right: segmented and filtered densities for the same area of the whole tomogram rotated by 45°. Numbers mark the same particles on two tomogram representations.
(D) Negative stain EM tomography of mouse Cavin1 complexes following crosslinking and detergent treatment. Tomograms are shown in Movies S1 and S2. Black particles are fiducial gold used to perform accurate tomographic modeling.
(E) Magnified views of highlighted regions from (D). The left image in each horizontal pair shows the original image, middle shows the manual segmentation of cavin rod elements in that image, and right shows the segmented structures.
(F) Quantification of the dimensions of the smallest straight rod particles from (D). Error bar represents SD.
(G) Comparison of linear sizes of identified cavin rods with the HR1 domain crystal structure and putative HR2 domains of mouse Cavin1.
(H) Quantification of the period of rod lattice. Plotted are pixel intensity profiles drawn perpendicularly to main axis of rods arranged in lattices in (D).

This work was supported by grants from the National Health and Medical Research Council of Australia (NHMRC) (grant number APP569542 to R.G.P.; grant number APP1037320 to R.G.P. and K.A.) and the Australian Research Council (ARC) (grant number DP120101298 to B.M.C.) and partly by the Australian Research Council Centre of Excellence in Convergent Bio-Nano Science and Technology (project number CE140100036). R.G.P. is supported by an NHMRC Senior Principal Research Fellowship from the NHMRC (APP1058565), K.A. by an ARC Future Fellowship (FT0991611), and B.M.C. by an ARC Future Fellowship (FT100100027).

Received: July 1, 2014
Revised: August 29, 2014
Accepted: October 2, 2014
Published: November 13, 2014

REFERENCES

Bastiani, M., Liu, L., Hill, M.M., Jedrychowski, M.P., Nixon, S.J., Lo, H.P., Abankwa, D., Luetterforst, R., Fernandez-Rojo, M., Breen, M.R., et al. (2009). MURC/Cavin-4 and cavin family members form tissue-specific caveolar complexes. J. Cell Biol. *185*, 1259–1273.

Breen, M.R., Camps, M., Carvalho-Simoes, F., Zorzano, A., and Pilch, P.F. (2012). Cholesterol depletion in adipocytes causes caveolae collapse concomitant with proteosomal degradation of cavin-2 in a switch-like fashion. PLoS ONE *7*, e34516.

Burgener, R., Wolf, M., Ganz, T., and Baggiolini, M. (1990). Purification and characterization of a major phosphatidylserine-binding phosphoprotein from human platelets. Biochem. J. *269*, 729–734.

Ciani, B., Bjelic, S., Honnappa, S., Jawhari, H., Jaussi, R., Payapilly, A., Jowitt, T., Steinmetz, M.O., and Kammerer, R.A. (2010). Molecular basis of coiled-coil oligomerization-state specificity. Proc. Natl. Acad. Sci. USA *107*, 19850–19855.

Conners, R., Hill, D.J., Borodina, E., Agnew, C., Daniell, S.J., Burton, N.M., Sessions, R.B., Clarke, A.R., Catto, L.E., Lammie, D., et al. (2008). The Moraxella adhesin UspA1 binds to its human CEACAM1 receptor by a deformable trimeric coiled-coil. EMBO J. *27*, 1779–1789.

Fernandez, I., Ying, Y., Albanesi, J., and Anderson, R.G. (2002). Mechanism of caveolin filament assembly. Proc. Natl. Acad. Sci. USA *99*, 11193–11198.

Folta-Stogniew, E., and Williams, K.R. (1999). Determination of molecular masses of proteins in solution: Implementation of an HPLC size exclusion chromatography and laser light scattering service in a core laboratory. J. Biomol. Tech. *10*, 51–63.

Fra, A.M., Williamson, E., Simons, K., and Parton, R.G. (1995). De novo formation of caveolae in lymphocytes by expression of VIP21-caveolin. Proc. Natl. Acad. Sci. USA *92*, 8655–8659.

Fujita, A., Cheng, J., Tauchi-Sato, K., Takenawa, T., and Fujimoto, T. (2009). A distinct pool of phosphatidylinositol 4,5-bisphosphate in caveolae revealed by a nanoscale labeling technique. Proc. Natl. Acad. Sci. USA *106*, 9256–9261.

Gambin, Y., Ariotti, N., McMahon, K.A., Bastiani, M., Sierecki, E., Kovtun, O., Polinkovsky, M.E., Magenau, A., Jung, W., Okano, S., et al. (2014). Single-molecule analysis reveals self assembly and nanoscale segregation of two distinct cavin subcomplexes on caveolae. eLife *3*, e01434.

Gustincich, S., and Schneider, C. (1993). Serum deprivation response gene is induced by serum starvation but not by contact inhibition. Cell growth & differentiation: the molecular biology journal of the American Association for Cancer Research *4*, 753–760.

Gustincich, S., Vatta, P., Goruppi, S., Wolf, M., Saccone, S., Della Valle, G., Baggiolini, M., and Schneider, C. (1999). The human serum deprivation response gene (SDPR) maps to 2q32-q33 and codes for a phosphatidylserine-binding protein. Genomics *57*, 120–129.

Hailstones, D., Sleer, L.S., Parton, R.G., and Stanley, K.K. (1998). Regulation of caveolin and caveolae by cholesterol in MDCK cells. J. Lipid Res. *39*, 369–379.

Hansen, C.G., and Nichols, B.J. (2010). Exploring the caves: cavins, caveolins and caveolae. Trends Cell Biol. *20*, 177–186.

Hansen, C.G., Bright, N.A., Howard, G., and Nichols, B.J. (2009). SDPR induces membrane curvature and functions in the formation of caveolae. Nat. Cell Biol. *11*, 807–814.

Hansen, C.G., Shvets, E., Howard, G., Riento, K., and Nichols, B.J. (2013). Deletion of cavin genes reveals tissue-specific mechanisms for morphogenesis of endothelial caveolae. Nat. Commun. *4*, 1831.

Hartmann, M.D., Ridderbusch, O., Zeth, K., Albrecht, R., Testa, O., Woolfson, D.N., Sauer, G., Dunin-Horkawicz, S., Lupas, A.N., and Alvarez, B.H. (2009). A coiled-coil motif that sequesters ions to the hydrophobic core. Proc. Natl. Acad. Sci. USA *106*, 16950–16955.

Hartmann, M.D., Grin, I., Dunin-Horkawicz, S., Deiss, S., Linke, D., Lupas, A.N., and Hernandez Alvarez, B. (2012). Complete fiber structures of complex trimeric autotransporter adhesins conserved in enterobacteria. Proc. Natl. Acad. Sci. USA *109*, 20907–20912.

Hayer, A., Stoeber, M., Bissig, C., and Helenius, A. (2010). Biogenesis of caveolae: stepwise assembly of large caveolin and cavin complexes. Traffic *11*, 361–382.

Hill, M.M., Bastiani, M., Luetterforst, R., Kirkham, M., Kirkham, A., Nixon, S.J., Walser, P., Abankwa, D., Oorschot, V.M., Martin, S., et al. (2008). PTRF-Cavin, a conserved cytoplasmic protein required for caveola formation and function. Cell *132*, 113–124.

Holm, L., and Rosenström, P. (2010). Dali server: conservation mapping in 3D. Nucleic Acids Res. *38*, W545-9.

Humphrey, S.J., Yang, G., Yang, P., Fazakerley, D.J., Stöckli, J., Yang, J.Y., and James, D.E. (2013). Dynamic adipocyte phosphoproteome reveals that Akt directly regulates mTORC2. Cell Metab. *17*, 1009–1020.

Izumi, Y., Hirai, Si., Tamai, Y., Fujise-Matsuoka, A., Nishimura, Y., and Ohno, S. (1997). A protein kinase Cdelta-binding protein SRBC whose expression is induced by serum starvation. J. Biol. Chem. *272*, 7381–7389.

Kovtun, O., Mureev, S., Jung, W., Kubala, M.H., Johnston, W., and Alexandrov, K. (2011). Leishmania cell-free protein expression system. Methods *55*, 58–64.

Lanzafame, A.A., Turnbull, L., Amiramahdi, F., Arthur, J.F., Huynh, H., and Woodcock, E.A. (2006). Inositol phospholipids localized to caveolae in rat heart are regulated by alpha1-adrenergic receptors and by ischemia-reperfusion. Am. J. Physiol. Heart Circ. Physiol. *290*, H2059–H2065.

Liu, L., Brown, D., McKee, M., Lebrasseur, N.K., Yang, D., Albrecht, K.H., Ravid, K., and Pilch, P.F. (2008). Deletion of Cavin/PTRF causes global loss of caveolae, dyslipidemia, and glucose intolerance. Cell Metab. *8*, 310–317.

Ludwig, A., Howard, G., Mendoza-Topaz, C., Deerinck, T., Mackey, M., Sandin, S., Ellisman, M.H., and Nichols, B.J. (2013). Molecular composition and ultrastructure of the caveolar coat complex. PLoS Biol. *11*, e1001640.

Matsuoka, K., and Schekman, R. (2000). The use of liposomes to study COPII- and COPI-coated vesicle formation and membrane protein sorting. Methods *20*, 417–428.

McMahon, K.A., Zajicek, H., Li, W.P., Peyton, M.J., Minna, J.D., Hernandez, V.J., Luby-Phelps, K., and Anderson, R.G. (2009). SRBC/cavin-3 is a caveolin adapter protein that regulates caveolae function. EMBO J. *28*, 1001–1015.

Mineo, C., Ying, Y.S., Chapline, C., Jaken, S., and Anderson, R.G. (1998). Targeting of protein kinase Calpha to caveolae. J. Cell Biol. *141*, 601–610.

Mureev, S., Kovtun, O., Nguyen, U.T., and Alexandrov, K. (2009). Species-independent translational leaders facilitate cell-free expression. Nat. Biotechnol. *27*, 747–752.

Murray, D.H., and Tamm, L.K. (2009). Clustering of syntaxin-1A in model membranes is modulated by phosphatidylinositol 4,5-bisphosphate and cholesterol. Biochemistry *48*, 4617–4625.

Palade, G.E. (1953). Fine structure of blood capillaries. J. Appl. Physiol. *24*, 1424.

Parton, R.G., and del Pozo, M.A. (2013). Caveolae as plasma membrane sensors, protectors and organizers. Nat. Rev. Mol. Cell Biol. *14*, 98–112.

Peters, K.R., Carley, W.W., and Palade, G.E. (1985). Endothelial plasmalemmal vesicles have a characteristic striped bipolar surface structure. J. Cell Biol. *101*, 2233–2238.

Rothberg, K.G., Heuser, J.E., Donzell, W.C., Ying, Y.S., Glenney, J.R., and Anderson, R.G. (1992). Caveolin, a protein component of caveolae membrane coats. Cell *68*, 673–682.

Sinha, B., Köster, D., Ruez, R., Gonnord, P., Bastiani, M., Abankwa, D., Stan, R.V., Butler-Browne, G., Vedie, B., Johannes, L., et al. (2011). Cells respond to mechanical stress by rapid disassembly of caveolae. Cell *144*, 402–413.

Steinmetz, M.O., Jelesarov, I., Matousek, W.M., Honnappa, S., Jahnke, W., Missimer, J.H., Frank, S., Alexandrescu, A.T., and Kammerer, R.A. (2007). Molecular basis of coiled-coil formation. Proc. Natl. Acad. Sci. USA *104*, 7062–7067.

Walser, P.J., Ariotti, N., Howes, M., Ferguson, C., Webb, R., Schwudke, D., Leneva, N., Cho, K.J., Cooper, L., Rae, J., et al. (2012). Constitutive formation of caveolae in a bacterium. Cell *150*, 752–763.

Westermann, M., Steiniger, F., and Richter, W. (2005). Belt-like localisation of caveolin in deep caveolae and its re-distribution after cholesterol depletion. Histochem. Cell Biol. *123*, 613–620.

Yamada, E. (1955). The fine structure of the gall bladder epithelium of the mouse. J. Biophys. Biochem. Cytol. *1*, 445–458.

Yang, P., Patrick, E., Tan, S.X., Fazakerley, D.J., Burchfield, J., Gribben, C., Prior, M.J., James, D.E., and Hwa Yang, Y. (2014). Direction pathway analysis of large-scale proteomics data reveals novel features of the insulin action pathway. Bioinformatics *30*, 808–814.

Zhang, J., Xiao, P., and Zhang, X. (2009). Phosphatidylserine externalization in caveolae inhibits Ca2+ efflux through plasma membrane Ca2+-ATPase in ECV304. Cell Calcium *45*, 177–184.